Journal of Circuits, Systems, and Computers
Vol. 19, No. 4 (2010) 773–785

DOI: 10.1142/S0218126610006438

World Scientific
www.worldscientific.com

CONTINUATION ANALYSIS OF A PHASE/QUADRATURE ELECTRONIC OSCILLATOR

FEDERICO BIZZARRI*, DANIELE LINARO† and MARCO STORACE‡

Biophysical and Electronic Engineering Department,
University of Genoa, Via Opera Pia 11a, I-16145, Genoa, Italy
**federico.bizzarri@unige.it*
†*daniele.linaro@unige.it*
‡*marco.storace@unige.it*

ANGELO BRAMBILLA

Politecnico di Milano, Dipartimento di Elettronica e Informazione,
p.za Leonardo da Vinci, 32, Milano, I-20133, Italy
brambill@elet.polimi.it

An RF phase-quadrature oscillator is analyzed. The designer "ensured" the phase-quadrature working condition through a suitable cross-coupled electrical connection between the two parts composing the complete oscillator. Through a detailed analysis of the dynamics of this oscillator, we show that device mismatch can lead to an unexpected stable working mode where the oscillator does not operate in a phase-quadrature condition. The proposed analysis has been first performed on a simplified model of the oscillator to allow the use of software packages for numerical continuation. The results of the analysis of the simplified oscillator dynamics have been then checked by means of accurate device models from a 65 nm RF technology library.

Keywords: Phase/quadrature oscillator; continuation; boundary value problem; bifurcation.

1. Introduction

In this paper we analyze the *structural stability* (i.e., the sensitivity to parameter variations) of a phase-quadrature oscillator obtained by suitably cross-coupling two identical oscillators (say, O_a and O_b).[1]

In the original paper, the circuit behavior has been explained only from a "phenomenological" standpoint but the phase-quadrature working condition is not ensured by any rigorous analytical approach.

Here, we use continuation methods and bifurcation analysis[2] to check the structural stability of the oscillator design. To this end, we study a simplified model of the oscillator, by checking *a posteriori* the analysis results through the circuit simulator

PAN[a] with accurate models of a 65 nm RF technology, that can be possibly adopted to implement on silicon the phase-quadrature oscillator.

Continuation methods allow one to translate the bifurcation analysis of steady state, either stationary (equilibrium points) or periodic (limit cycles), behaviors into the solution of an implicit algebraic equation which can be computed systematically. Hence, the bifurcation analysis is reduced to locating the zeroes of some functions, which can be found, with the desired precision, by using Newton-based algorithms. The reader is referred to Ref. 3 for a circuit-oriented treatment of this topic.

The structural stability (i.e., the robustness of the steady-state dynamical behavior with respect to parameter variations) of the oscillator is analyzed with respect to two bifurcation parameters: one governing the cross-coupling between O_a and O_b and one introducing a parameter mismatch between the oscillators. The cross-coupling is controlled by the designer through the width of suitable pairs of MOSFETs. The fabrication process mismatches many circuit parameters and we will focus on capacitors. Mismatches cannot be fully controlled by designers: they usually perform a set of Monte Carlo analyses to ensure that their design works properly. However, Monte Carlo analyses are very time consuming. In this paper, a more efficient approach is proposed. Part of the analysis carried out exploits in a standard way software packages for numerical continuation (MATCONT,[4] AUTO[5,6]). A second set of results has been obtained by defining a specific boundary value problem that is solved by using numerical continuation techniques.

Results provided by the continuation analysis of the simplified model and circuit simulations of the realistic model show good agreement. In particular, one of the results of the analysis is the identification of a *synchronization region* (an "Arnol'd tongue") in the parameters plane. When the values of the cross-coupling and mismatch parameters identify points outside the *synchronization region*, the phase-quadrature oscillator works in a condition where O_a and O_b are neither synchronized nor in quadrature. Furthermore, the output shows a low-frequency beat due to two different working periods of O_a and O_b. It is shown that this behavior (extremely "dangerous" from the oscillator design standpoint) is present also in the accurate model of the phase-quadrature oscillator.

2. The Phase/Quadrature Oscillator

The circuit shown in Fig. 1 models a phase-quadrature oscillator working at about 5 GHz.[1] It is a redesign of a previous circuit[7] where Millar's approach[8] has been exploited. In all these works[1,7,8] it has been shown that the phase-quadrature working condition can be met by suitably cross-coupling two identical oscillators. In the considered circuit, the cross-coupling is realized through two pairs (`n3a` and `n4a`,

[a] A binary version of the PAN simulator running under the LINUX operating system is available at the URL: http://brambilla.elet.polimi.it.

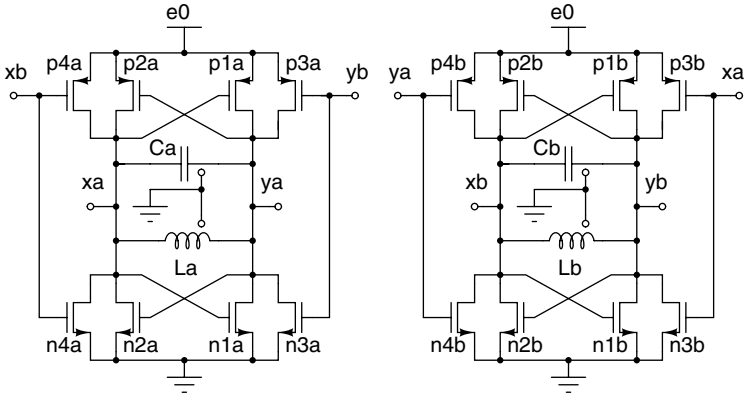

Fig. 1. Schematic of the phase/quadrature oscillator, obtained by cross-coupling oscillators O_a (left) and O_b (right).

`p3a` and `p4a`) of NMOS and PMOS transistors, respectively, belonging to O_a. These transistors are driven by the output voltage of O_b. The same situation applies to O_b that, in turn, is driven by O_a, with the driving terminals exchanged. The authors claim that this kind of connection damps the in-phase (in-opposition) working mode of the phase-quadrature oscillator by draining energy from the resonator of either O_a or O_b. Energy draining damps the amplitude of the oscillations until the oscillator is switched off; this oscillator then restarts in the quadrature condition, which sustains oscillations. The cross-coupling coefficient is chosen[1] by setting the widths of the cross-coupling MOSFETs equal to 1/3 of the other MOSFETs' widths. The "phenomenological" explanation and the choice of parameters have not been proven by any rigorous analytical approach; we believe that the main reason is the extreme complexity of the mathematical analysis.

We simulated this oscillator by employing elements from a 65 nm RF technology. In the technology model file, the MOSFETs are modeled through a subcircuit that accounts for high-frequency effects and parasitics due to routing. This subcircuit is shown in Fig. 2(a). The resonant circuit is composed of MOM (metal-oxide-metal) capacitors (`Ca` and `Cb`) and of spiral inductors (`La` and `Lb`). The MOMs are modeled through the subcircuit shown in Fig. 2(b). The nodes `A` and `B` are connected to the nodes `xa`, `ya` and `xb`, `yb` in the schematic shown in Fig. 1. Capacitors `Cpa` and `Cpb` model the parasitic capacitances between the two MOM metal plates and the substrate. The `Cmom` capacitor is nonlinear and voltage controlled. The `P` node of the MOM subcircuit is connected to ground in the schematic of Fig. 1. Inductors `La` and `Lb` are modeled by the subcircuit shown in Fig. 2(c). Due to parasitic capacitances, each inductor resonates at a frequency of some tens of GHz, depending on its physical dimensions. As for the MOMs, the nodes `Top` and `Bottom` in the subcircuit are connected to the nodes `xa`, `ya` and `xb`, `yb` in the schematic of Fig. 1; the node labeled as `Gnode` is connected to ground.

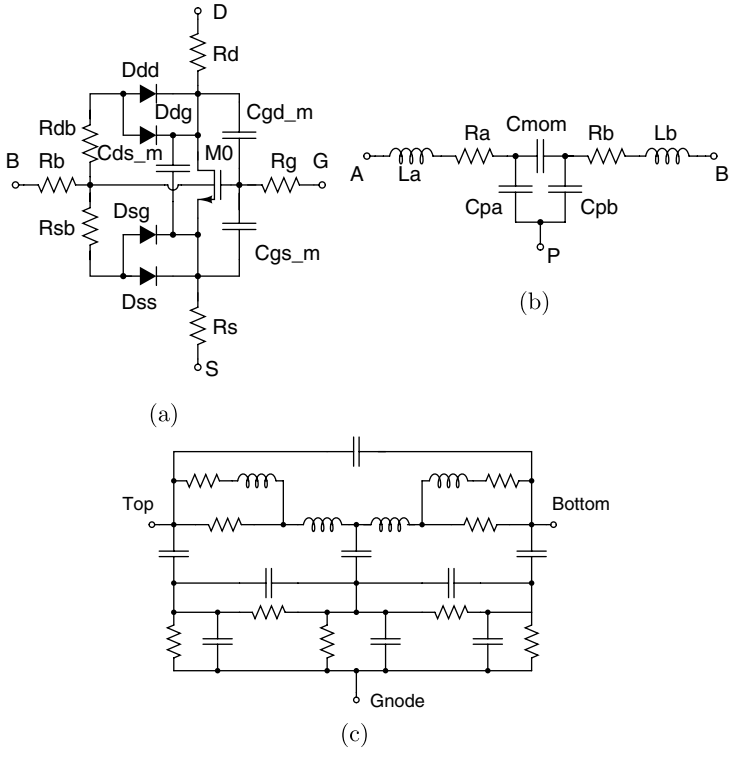

Fig. 2. (a) equivalent model of the RF MOSFET of the 65 nm technology library, (b) equivalent model of the MOM capacitor, (c) equivalent model of the spiral inductor.

By considering the complete schematic (not shown due to space reasons) of the phase-quadrature oscillator, one can see that the system order (also taking into account parasitic nonlinear capacitances of the MOSFETs) is quite high and thus the circuit may show very "rich" dynamics. Indeed, the complete netlist contains 215 nodes, 114 capacitors (excluding parasitic capacitances of MOSFETs), and 40 inductors. The large number of capacitors is due to the parallel connection of several MOMs. Nevertheless, we expect that the "main" dynamical behaviors be determined by the two LC resonators and by the oscillators' coupling.

In the following, we propose an equivalent simplified model of the phase-quadrature oscillator (shown in Fig. 3), which is suitable for a numerical analysis using continuations methods. We employed simplified versions of both MOSFET models (LEVEL1 of SPICE[9]) and passive components. For the NMOS transistor, the drain/source current is modeled as follows:

$$\begin{aligned} \imath_{ds,n}(v_{gs}, v_{ds}, K, V_t) \;=\; & u(v_{gs}-V_t)K\{u(v_{gs}-V_t-v_{ds})[(v_{gs}-V_t)^2 - v_{ds}]v_{ds} \\ & + [1-u(v_{gs}-V_t-v_{ds})](v_{gs}-V_t)^2\}, \end{aligned} \tag{1}$$

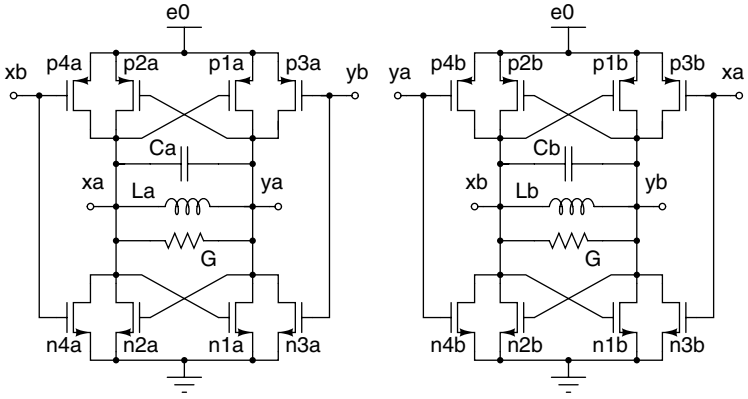

Fig. 3. The simplified model of the phase/quadrature oscillator. Passive elements are ideal and the MOSFET model is the LEVEL1 of SPICE.

where $K = \frac{1}{2}\mu c_{ox}\frac{W}{L}$ defines the maximum drain/source current, V_t is the threshold voltage and

$$u(x) = \begin{cases} 1 & \text{if } x > 0 \\ 0 & \text{otherwise} \end{cases}$$

Passive devices have been considered as ideal: more accurate models from a submicron technology library for RF applications have not been employed to drastically reduce the number of state variables. The quality factor of the integrated inductors has been modeled by connecting in parallel to each inductor the conductance `G`. With these simplifications, we can write Kirchhoff's equations as follows ($\imath_a$ and $\imath_b$ are the inductor currents, x_a and x_b are the node voltages for nodes `xa` and `xb`, respectively):

$$\begin{cases} -C\left(\dfrac{dx_a}{dt} - \dfrac{dy_a}{dt}\right) - \imath_a + \imath_{n1a}(x_a, y_a) + \imath_{p1a}(x_a - e_0, y_a - e_0) \\ \qquad + \imath_{n3a}(y_b, y_a) + \imath_{p3a}(y_b - e_0, y_a - e_0) - G(x_a - y_a) = 0 \\ C\left(\dfrac{dx_a}{dt} - \dfrac{dy_a}{dt}\right) + \imath_a + \imath_{n2a}(y_a, x_a) + \imath_{p2a}(y_a - e_0, x_a - e_0) \\ \qquad + \imath_{n4a}(x_b, x_a) + \imath_{p4a}(x_b - e_0, x_a - e_0) + G(x_a - y_a) = 0 \\ \qquad L\dfrac{d\imath_a}{dt} - x_a + y_a = 0 \\ -C\left(\dfrac{dx_b}{dy} - \dfrac{dy_b}{dt}\right) - \imath_b + \imath_{n1b}(x_b, y_b) + \imath_{p1b}(x_b - e_0, y_b - e_0) \\ \qquad + \imath_{n3b}(x_a, y_b) + \imath_{p3b}(x_a - e_0, y_b - e_0) - G(x_b - y_b) = 0 \\ C\left(\dfrac{dx_b}{dt} - \dfrac{dy_b}{dt}\right) + \imath_b + \imath_{n2b}(y_b, x_b) + \imath_{p2b}(y_b - e_0, x_b - e_0) \\ \qquad + \imath_{n4b}(y_a, x_b) + \imath_{p4b}(y_a - e_0, x_b - e_0) + G(x_b - y_b) = 0 \\ \qquad L\dfrac{d\imath_b}{dt} - x_b + y_b = 0\,, \end{cases} \tag{2}$$

where

$$\begin{aligned}
\imath_{n1a}(x,y) &= \imath_{n1b}(x,y) = \imath_{n2a}(x,y) = \imath_{n2b}(x,y) = \imath_{ds,n}(x,y,K_n,V_{tn})\,,\\
\imath_{p1a}(x,y) &= \imath_{p1b}(x,y) = \imath_{p2a}(x,y) = \imath_{p2b}(x,y) = \imath_{ds,p}(x,y,K_p,V_{tp})\,,\\
\imath_{n3a}(x,y) &= \imath_{n3b}(x,y) = \imath_{n4a}(x,y) = \imath_{n4b}(x,y) = \imath_{ds,n}(x,y,\alpha K_n,V_{tn})\,,\\
\imath_{p3a}(x,y) &= \imath_{p3b}(x,y) = \imath_{p4a}(x,y) = \imath_{p4b}(x,y) = \imath_{ds,p}(x,y,\alpha K_p,V_{tp})
\end{aligned}$$

with $K_n = 100\,\mu\mathrm{AV}^{-2}$, $V_{tn} = 0.5\,\mathrm{V}$, $K_p = -100\,\mu\mathrm{AV}^{-2}$, $V_{tp} = -0.5\,\mathrm{V}$ and $L = 2\,\mathrm{nH}$, $C = 0.126\,\mathrm{pF}$, $e_0 = 3.3\,\mathrm{V}$.

By algebraic handling of Eqs. (2) and by defining $V_n = x_n - y_n,\ n = \{a,b\}$, we obtain

$$\begin{cases}
\imath_{n1a}(x_a, x_a - V_a) + \imath_{p1a}(x_a - e_0, x_a - V_a - e_0)\\
+\imath_{n3a}(x_b - V_b, x_a - V_a) + \imath_{p3a}(x_b - V_b - e_0, x_a - V_a - e_0)\\
+\imath_{n2a}(x_a - V_a, x_a) + \imath_{p2a}(x_a - V_a - e_0, x_a - e_0)\\
+\imath_{n4a}(x_b, x_a) + \imath_{p4a}(x_b - e_0, x_a - e_0) = 0\\
\imath_{n1b}(x_b, x_b - V_b) + \imath_{p1b}(x_b - e_0, x_b - V_b - e_0)\\
+\imath_{n3b}(x_a, x_b - V_b) + \imath_{p3b}(x_a - e_0, x_b - V_b - e_0)\\
+\imath_{n2b}(x_b - V_b, x_b) + \imath_{p2b}(x_b - V_b - e_0, x_b - e_0)\\
+\imath_{n4b}(x_a - V_a, x_b) + \imath_{p4b}(x_a - V_a - e_0, x_b - e_0) = 0
\end{cases} \tag{3}$$

whose solutions are the node voltages x_a and x_b. Therefore, the equations employed to perform the continuation analysis are

$$\begin{cases}
-C\dfrac{dV_a}{dt} - \imath_a + \imath_{n1a}(x_a, y_a) + \imath_{p1a}(x_a - e_0, y_a - e_0)\\
\quad + \imath_{n3a}(y_b, y_a) + \imath_{p3a}(y_b - e_0, y_a - e_0) - GV_a = 0\\
\qquad\qquad L\dfrac{d\imath_a}{dt} - V_a = 0\\
-C\dfrac{dV_b}{dt} + \imath_b + \imath_{n1b}(x_b, y_b) + \imath_{p1b}(x_b - e_0, y_b - e_0)\\
\quad + \imath_{n3b}(x_a, y_b) - \imath_{p3b}(x_a - e_0, y_b - e_0) - GV_b = 0\\
\qquad\qquad L\dfrac{d\imath_b}{dt} - V_b = 0\,.
\end{cases} \tag{4}$$

Before describing the analysis and the obtained results, we introduce some remarks. As stated above, the two implemented oscillators O_a and O_b are not identical: for example, uncertainties in the fabrication process and parasitics introduce mismatches between the values of the capacitors/inductors composing the resonant circuit and of the tuning MOMs capacitors. In the simplified model, the two resonant capacitors have been mismatched by introducing the parameter ϵ: $C_a = C$ and $C_b = (1+\epsilon)C$.

Another circuit parameter of a certain interest is the size of the transistors making up the cross-coupling circuit. The width of these transistors is equal to 1/3 of those composing the LC-tank oscillator,[1] but, to the best of the authors' knowledge, without providing any justification. In the following, we shall refer to this ratio as the coupling parameter α.

3. Results of the Analysis

To evaluate the structural stability of the oscillator dynamics with respect to variations of one or both of the chosen bifurcation parameters, we focused on two targets:

- robustness of the quadrature behavior with respect to the capacitors' mismatch
- identification of the region corresponding to quadrature behavior on the plane (α, ϵ).

This kind of analysis provides the designer with some elements to ensure a correct behavior of the oscillator. Of course, one can change the bifurcation parameters and carry out an analysis more tailored to specific design interests.

By normalizing the oscillation period, the quadrature condition used in the continuation analysis is expressed as

$$\phi = \int_0^1 V_a V_b \, dt \,. \tag{5}$$

Equation (5) shows that $\phi = 0$ when the oscillator works in the quadrature condition.

3.1. *Analysis with varying ϵ*

To start with, we set the coupling coefficient to $\alpha = 0.05$ and analyze the oscillator behavior with respect to the capacitors' mismatch. To this end, we start from a stable periodic solution numerically obtained for $\epsilon = 0$ (no mismatch) and we continue it by varying ϵ. Figure 4 (left panel) shows the value of ϕ versus ϵ. Of course, we have symmetry with respect to the axes $\epsilon = 0$ and $\phi = 0$: perfect quadrature between V_a and V_b is achieved only in the center of the "eight-shaped" curve (i.e., in this point the phase mismatch between V_a and V_b is exactly 90°). Indeed, as ϕ is no longer equal to 0, a perfect quadrature working condition is lost and the phase mismatch between V_a and V_b is equal to $|\phi|$. Along the "eight-shaped" curve, V_a and V_b are synchronized (i.e., share the same frequency and amplitude, but not the same phase) on a limit cycle. Along the solid part of the curve the limit cycle is stable, whereas along the dashed portions it is unstable. For values of ϵ that lie outside the "eight-shaped" curve, the oscillators O_a and O_b show different working periods, which yield a "low-frequency" beat (i.e., a low-frequency amplitude modulation) in the outputs of the phase-quadrature oscillator. Therefore, V_a and V_b are no longer synchronized and

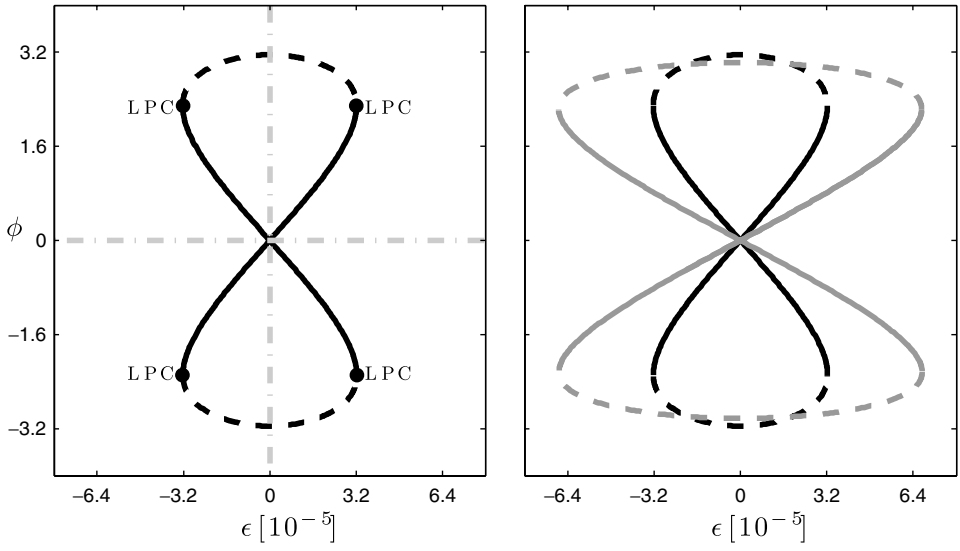

Fig. 4. Continuation (with AUTO2000) with respect to ϵ of a cycle for $\alpha = 0.05$ (left panel), $\alpha = 0.05$ (black curve) and $\alpha = 0.95$ (grey curve) (right panel).

they correspond to a stable torus. This suggests the presence of an "Arnol'd tongue",[10] whose presence will be commented on in the next subsection.

Figure 4 (left panel) points out the presence of fold of cycles bifurcations (at the labels LPC), where the stable cycle (solid line) collides with an unstable cycle (dashed line). Owing to the system symmetries, we can conclude that we have only one stable solution.

By fixing the coupling coefficient to different values, we obtain very similar results, the only significant change being the width of the obtained "eight", as shown in Fig. 4 (right panel).

3.2. *Analysis in the* (ϵ, α) *plane*

By continuing the fold of cycles bifurcations described in the previous section, we obtain the Arnol'd tongue partially shown in Fig. 5;[b] inside the tongue the oscillator works in an approximate quadrature condition with different relative phases (different ϕ), whereas outside of the tongue the quadrature condition is completely lost and the presence of a torus can be observed.

3.3. *Analysis in the* (α, f, C) *space*

Once we have obtained, by varying ϵ and for a given pair (α, C), a satisfying value of ϕ, we can obtain by continuation the locus of points with the same value of ϕ in the

[b] The computation of Arnol'd tongues tips may be critical[11] and is out of the scopes of this paper.

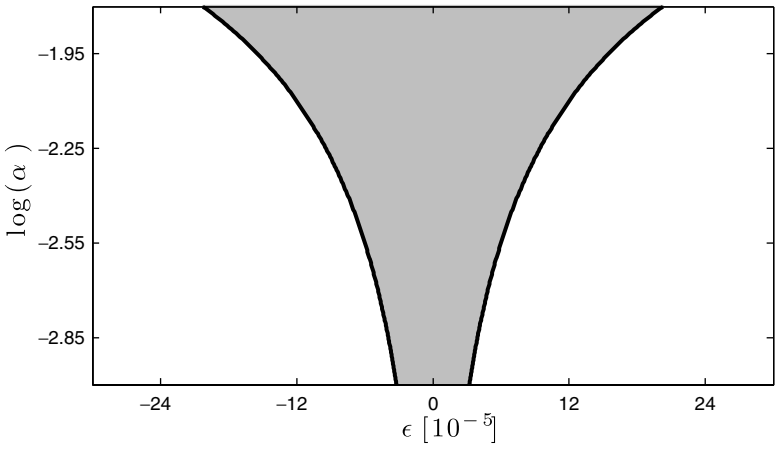

Fig. 5. Arnol'd tongue (grey region) obtained by continuing two fold of cycles bifurcations (labels LPC in Fig. 4).

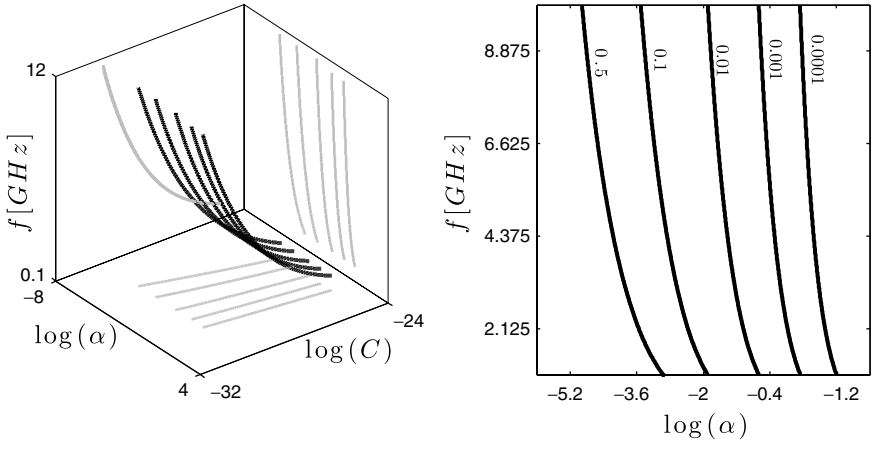

Fig. 6. Loci of points with the same value of ϕ in the parameter space (α, f, C) (left panel). Projections of the loci on the plane (α, f).

parameter space spanned by (α, f, C) (details about the mathematical definition of the continuation problem can be found in Appendix A). So doing, a designer is quite simply able to locate the combinations of cross-coupling, working frequency, and capacitance ensuring a correct behavior of the oscillator.

4. Validation of the Results

The obtained dynamical behaviors have been verified in some specific working conditions with the accurate models of a 65 nm RF technology. The first condition

considered is $\alpha = 1/3$ and $\epsilon = 0.02$ (a 2% device mismatch). These working conditions lead to synchronization; after an initial setup phase, the phase-quadrature oscillator gives almost in quadrature output voltages, describing a limit cycle in the state space $(V_a, V_b, \imath_a, \imath_b)$. The numerically computed largest modulus of the Floquet multipliers is 0.99526 and the second largest is 0.87228; this shows that the limit cycle is stable. The phase relation between the output voltages is 101°. Figure 7 displays a portion of the simulated output waveforms that shows the transition from "in-phase" unstable working condition to "stable" quadrature working condition. The analogue circuit simulator PAN has been employed to perform simulations.

The synchronization of V_a and V_b can also be checked by resorting to a Poincaré section defined as the locus of the maxima of a state variable. The intersections of a trajectory with this section can be easily obtained by sampling results at the time instants corresponding to the maxima of the chosen state variable, that in our case is the current $\imath_a$.

Figure 8 (left panel) shows the Poincaré section samples of the simulated V_a waveform. After the initial settling of the phase-quadrature oscillator, the V_a samples converge to a constant value, meaning that the only characteristic frequency is the oscillation frequency.

Since the silicon area occupied by the MOSFETs of the LC-tank oscillator is considerable, the choice of reducing their area is not negligible. Therefore, the same kind of simulations have been repeated with a "weaker" coupling coefficient that sets the

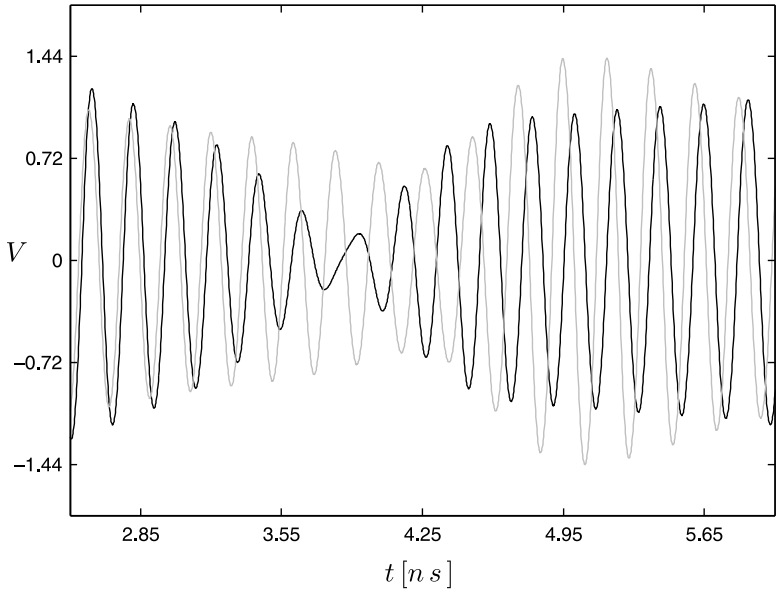

Fig. 7. Portion of the output voltages $V_a(t)$ (black line) and $V_b(t)$ (gray line) of the 65 nm phase-quadrature oscillator.

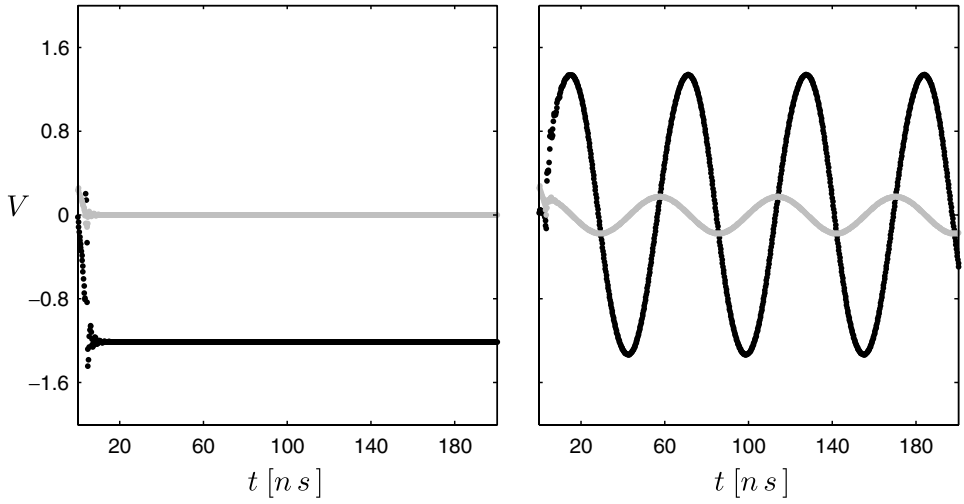

Fig. 8. Samples of $V_a(t)$ (black dots) and of $V_b(t)$ (gray dots) at the intersections with the Poincaré section (see text). Synchronized case (left panel) and unsynchronized case (right panel).

working point of the oscillator outside the Arnol'd tongue. By observing the result shown in Fig. 8 (right panel), we can see that the values assumed by the V_a samples oscillate with period close to 55.72 ns. Since the two oscillators are not synchronized and have different values of the tuning capacitors (due to mismatch) they work at "slightly" different frequencies. This difference originates beats that are spaced in time by about 55.72 ns: this corresponds to a frequency of about 18 MHz.

5. Conclusions

In this paper we have shown through a case study that continuation techniques can be useful (even if their use may be quite complex) for the analysis/design of electronic oscillators. The considered phase-quadrature oscillator has been modeled by a simplified set of equations and then analyzed through numerical continuation. The obtained results have been qualitatively confirmed by simulations with the accurate models of a 65 nm RF technology.

Appendix A

In order to obtain the curves reported in Fig. 6, it is necessary to define a proper periodic Boundary Value Problem (BVP). Once we have obtained, by varying ϵ and for a given pair (α, C), a limit cycle characterized by a satisfying value of ϕ, this can be used as a starting solution for the BVP and can be continued in three parameters by resorting to AUTO.[5,6] The BVP is defined by the $N = 4$ state equations

(normalized by the oscillation period $T = \frac{1}{f}$) governing the oscillator dynamics

$$\begin{cases} \dfrac{dV_a}{dt} = TF_1(V_a, \imath_a, V_b, \imath_b) \\ \dfrac{d\imath_a}{dt} = TF_2(V_a, \imath_a, V_b, \imath_b) \\ \dfrac{dV_b}{dt} = TF_3(V_a, \imath_a, V_b, \imath_b) \\ \dfrac{d\imath_a}{dt} = TF_4(V_a, \imath_a, V_b, \imath_b) \end{cases} \tag{A.1}$$

with four periodic boundary conditions for the state variables ($BCND = 4$)

$$\begin{cases} V_a(0) = V_a(1) \\ \imath_a(0) = \imath_a(1) \\ V_b(0) = V_b(1) \\ \imath_b(0) = \imath_b(1) \end{cases} \tag{A.2}$$

and two integral conditions ($ICND = 2$): the standard integral phase condition adopted in limit cycle continuations[2] and the quadrature condition (5). Then, the number of free parameters ($BCND + ICND\text{-}N + 1$) is 3, corresponding to f and two system parameters, i.e., α and C.

References

1. M. Tiebout, Low-power low-phase-noise differentially tuned quadrature VCO design in standard CMOS, *IEEE J. Solid-State Circuits* **36** (2001) 1018−1024.
2. Y. Kuznetsov, *Elements of Applied Bifurcation Theory*, 3rd ed. (Springer-Verlag, New York, 2004).
3. G. Maggio, O. De Feo and M. Kennedy, Nonlinear analysis of the Colpitts oscillator and applications to design, *IEEE Trans. Circuits Syst. I* **46** (1999) 1118−1130.
4. A. Dhooge, W. Govaerts and Y. Kuznetsov, MATCONT: A MATLAB package for numerical bifurcation analysis of ODEs, *ACM Trans. Math. Software* **29** (2003) 141−164.
5. E. Doedel, R. Paffenroth, A. Champneys, T. Fairgrieve, Y. Kuznetsov, B. Sandstede and X. Wang, AUTO 2000: Continuation and bifurcation software for ordinary differential equations (with HomCont), Computer Science Department, Concordia University, Montreal, Quebec, Canada (2001).
6. E. Doedel, A. Champneys, F. Dercole, T. Fairgrieve, Y. Kuznetsov, B. Oldeman, R. Paffenroth, B. Sandstede, X. Wang and C. Zhang, AUTO-07p: Continuation and bifurcation software for ordinary differential equations, Computer Science Department, Concordia University, Montreal, Quebec, Canada (2007).
7. A. Rofougaran, J. Rael, M. Rofougaran and A. Abidi, A 900 MHz CMOS LC-oscillator with quadrature outputs, *Solid-State Circuits Conf. 1996. Digest of Technical Papers. 42nd ISSCC., 1996 IEEE Int.* February 1996, pp. 392−393.
8. D. Millar, A two-phase audio-frequency oscillator, *J. Institution of Electrical Engineers* **74** (1934) 365−371.

9. P. Antognetti and G. Massobrio, *Semiconductor Device Modeling with SPICE* (McGraw-Hill, Inc., 1988).
10. A. Pikovsky, M. Rosenblum and J. Kurths, *Synchronization. A Universal Concept in Nonlinear Sciences* (Cambridge University Press, Cambridge, 2001).
11. F. Schilder and B. Peckham, Computing Arnol'd tongue scenarios, *J. Computat. Phys.* **220** (2007) 932–951.